Local Versus Nonlocal Boundary-Layer Diffusion in a Global Climate Model

A. A. M. HOLTSLAG

Royal Netherlands Meteorological Institute (KNMI), De Bilt, the Netherlands

B. A. BOVILLE

National Center for Atmospheric Research, Boulder, Colorado*

(Manuscript received 26 December 1991, in final form 2 September 1992)

ABSTRACT

The results of a local and a nonlocal scheme for vertical diffusion in the atmospheric boundary layer are compared within the context of a global climate model. The global model is an updated version of the NCAR Community Climate Model (CCM2). The local diffusion scheme uses an eddy diffusivity determined independently at each point in the vertical, based on local vertical gradients of wind and virtual potential temperature, similar to the usual approach in global atmospheric models. The nonlocal scheme determines an eddy-diffusivity profile based on a diagnosed boundary-layer height and a turbulent velocity scale. It also incorporates nonlocal (vertical) transport effects for heat and moisture.

The two diffusion schemes are summarized, and their results are compared with independent radiosonde observations for a number of locations. The focus herein is on the temperature and humidity structure over ocean, where the surface temperatures are specified, since the boundary-layer scheme interacts strongly with the land-surface parameterization. Systematic differences are shown in global-climate simulations, with CCM2 using the two schemes. The nonlocal scheme transports moisture away from the surface more rapidly than the local scheme, and deposits the moisture at higher levels. The local scheme tends to saturate the lowest model levels unrealistically, which typically leads to clouds too low in the atmosphere.

The nonlocal scheme has been chosen for CCM2 because of its more comprehensive representation of the physics of boundary-layer transport in dry convective conditions.

1. Introduction

Turbulence in the atmospheric boundary layer (ABL) causes mixing of heat, moisture, momentum, and passive scalars. Global weather forecasting and climate models typically describe the turbulent mixing with an eddy diffusivity based on local gradients of wind and potential temperature. Such a so-called "local-K" approach is treated, for instance, by Louis (1979). Local-K theory may fail in the unstable boundary layer because the influence of large eddy transports is not accounted for (e.g., Wyngaard and Brost 1984; Holtslag and Moeng 1991), and entrainment effects are not treated in such an approach. This may affect the profiles of mean quantities, especially at locations where dry convection is of importance in the ABL.

A nonlocal ABL scheme is used in the NCAR Community Climate Model, Version 2 (CCM2). The nonlocal ABL scheme is based on the work by Troen and Mahrt (1986) and Holtslag et al. (1990). It utilizes an eddy-diffusivity profile and incorporates the nonlocal effects of transport by large eddies in a simplified manner (Holtslag and Moeng 1991). The latter represents the effects of dry convective plumes whose vertical scale is the depth of the boundary layer. Within this scheme, the boundary-layer depth is calculated explicitly. It also appears that the nonlocal diffusion scheme is more robust from a numerical point of view, because it is less sensitive to stability oscillations (Beljaars 1991).

A local-K scheme was used in the previous version of the CCM (CCM1). The nonlocal ABL scheme was selected for use in CCM2 because it represents important physical effects not contained in the local-K approach. The purpose of this paper is to document the nonlocal ABL scheme and to show its impact on the global-climate simulation produced by CCM2. The impact is determined by comparing with the results of an updated local-K approach. We focus on the results for temperature, specific humidity, and low clouds.

As an example, Fig. 1 shows the observed July mean vertical profiles of temperature and specific humidity of Truk Island (7.5°N, 151°E) in the tropics, compared to the simulated profiles produced using the local-K approach and the nonlocal approach (both approaches

* The National Center for Atmospheric Research is sponsored by the National Science Foundation.

Corresponding author address: Dr. Bert Holtslag, KNMI Research Department, P.O. Box 201, 3730 AE De Bilt, the Netherlands.

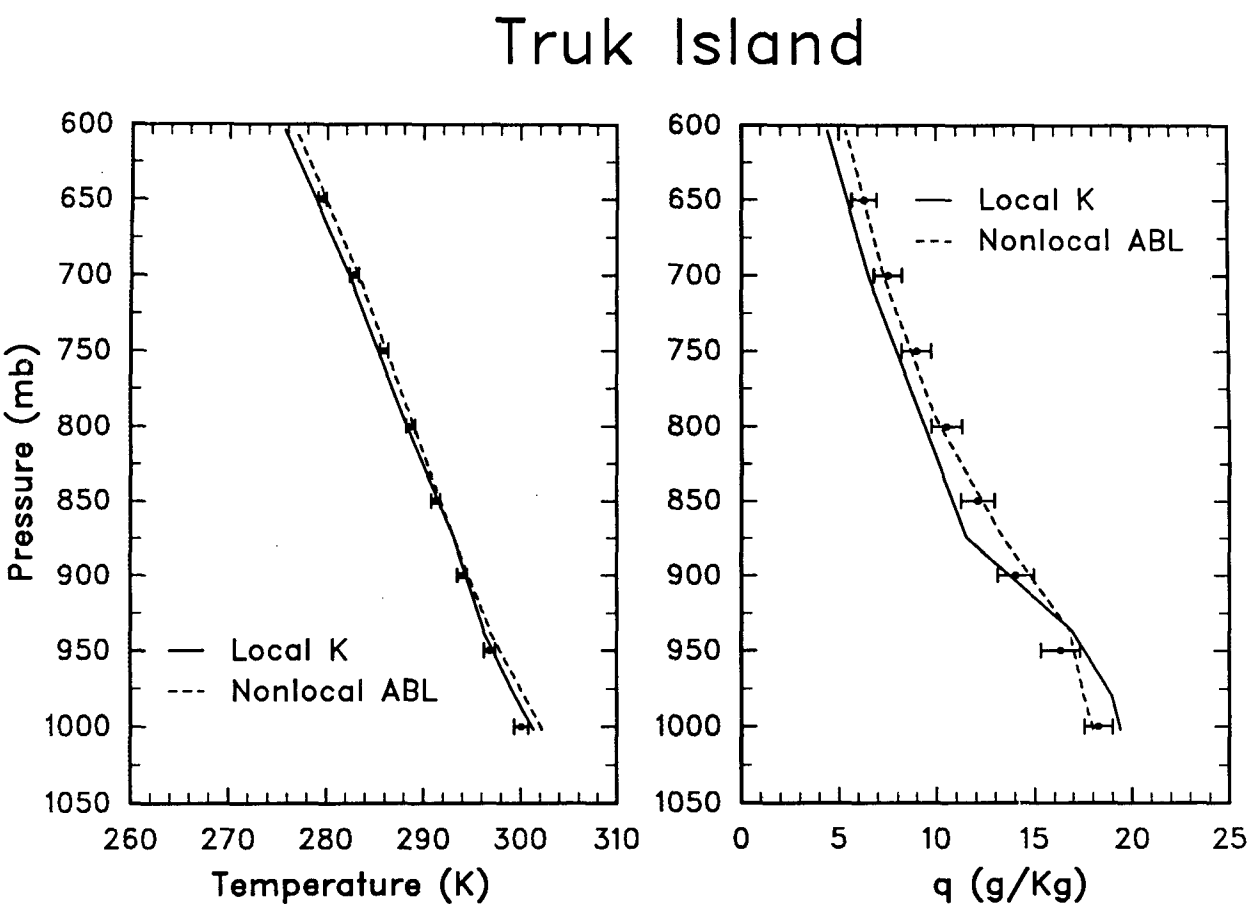

FIG. 1. The simulated mean July temperature (left panel) and specific humidity profile (right panel) in a grid point near Truk Island (7.5°N, 151°E), in comparison with radiosonde observations (dots with horizontal bars). Solid lines reflect results with CCM2 using the local diffusion scheme, and dashed lines refer to CCM2 with the nonlocal diffusion scheme.

will be described below). Note that over the oceans, the sea surface temperature is prescribed. Although the temperature profiles are similar, the vertical structure of the specific-humidity profile is much better simulated with the nonlocal ABL scheme in this case. With the local scheme, the total mixing of specific humidity is underestimated, resulting in too moist atmospheric levels near the surface. This will directly affect the surface fluxes of latent and sensible heat and may result in unrealistically large amounts of clouds at low levels. The fact that the temperature and specific humidity profiles are also influenced at heights above the ABL is due to the interaction of the nonlocal scheme with other parts of the model (in particular the convection scheme).

The basic model used for the simulations (CCM2), is briefly described in section 2. The local and nonlocal ABL schemes are described in section 3. The mean profiles produced by the ABL schemes are compared to radiosonde observations at a number of locations in section 4 (similar to Fig. 1). We also compare the outputs of the diffusion schemes for sample profiles in section 4. Section 5 contains a comparison of climate simulations using the two diffusion schemes. Here we also show results for the diagnosed boundary-layer height. Conclusions appear in section 6.

2. Description of CCM2 and experiments

a. General

CCM2 is the most recent version of the NCAR Community Climate Model. Although CCM2 is an outgrowth of the previous version (CCM1), described by Williamson et al. (1987), the model has been revised so extensively that only a few of the papers documenting the previous version are still relevant. The vertical coordinate, numerical approximations, and most physical parameterizations have been replaced, as summarized below. Detailed descriptions of changes to the model outside of the ABL scheme are beyond the scope of this paper and will be discussed in a number of forthcoming papers, most of which are still in preparation.

CCM2 is a global general circulation model that solves the primitive equations using the spectral-transform method in the horizontal and finite-difference approximations in the vertical. The large-scale transport of water now uses the three-dimensional semi-Lagrangian transport method described by Rasch and Williamson (1990) rather than the spectral method. The standard horizontal resolution of the model has been increased to T42 (as opposed to R15 in CCM1), employing a transform grid with a spacing of ~2.8° in both latitude and longitude. Momentum flux divergence by stationary gravity waves is parameterized following McFarlane (1987). A biharmonic (∇^4) horizontal diffusion operator is included as in CCM1, with coefficient 10^{16} m^4 s^{-1} as obtained by Boville (1991).

The standard vertical discretization employs 18 levels between the earth's surface and a rigid lid near 3 mb. CCM1 used 12 levels over approximately the same domain and much of the additional resolution has been concentrated near the surface. The σ coordinate has been replaced by the hybrid coordinate described by Simmons and Strüfing (1983). In the standard atmosphere, the lowest seven midpoint levels (where the mean quantities are calculated) are 992.5, 970.4, 929.3, 866.4, 786.5, 695.2, and 598.2 mb.

The shortwave radiation parameterization (Briegleb 1992) now uses the δ-Eddington method and incorporates both diurnal and annual cycles of insolation. The longwave radiation parameterization has also been updated (principally affecting the upper stratosphere). The cloud-fraction parameterization used for radiative purposes is a generalization of the method proposed by Slingo (1987). The diagnosed cloud fraction depends on relative humidity, vertical motion, static stability, and precipitation rate. Once clouds appear, their liquid-water concentration is specified as a function of latitude and height for the radiation calculations [similar to the description in Kiehl (1991)].

Land temperatures are predicted using a diffusion equation for the surface and three subsurface layers with differing heat capacities. Sea surface temperatures are prescribed by linear interpolation between climatological monthly mean values from Shea et al. (1990). The surface fluxes are calculated with the usual transfer coefficients between the surface and the first model level. Compared to CCM1 we have updated the stability dependence of the transfer coefficients. In the ABL, CCM2 incorporates the nonlocal diffusion scheme (see section 3b), while above the ABL, the local diffusion scheme is retained with a small value of 30 m for the length scale l_c in Eq. (3.2) of section 3a. A simple mass-flux scheme (Hack 1993) is used to represent both deep and shallow convection. The nonlocal ABL scheme provides a coupling between the surface fluxes and the convection parameterization by diagnosing turbulent temperature and moisture perturbations [see discussion in section 3b below Eq. (3.12)].

The parameterizations of the surface fluxes and of the vertical diffusion are described in more detail below because they are intimately coupled with the ABL parameterization.

b. *The surface fluxes*

The parameterized (kinematic) surface fluxes are given by

$$(\overline{w'u'})_0 = -C_M |V_1| u_1, \tag{2.1}$$

$$(\overline{w'v'})_0 = -C_M |V_1| v_1, \tag{2.2}$$

$$(\overline{w'\theta'})_0 = C_H |V_1| (\theta_0 - \theta_1), \tag{2.3}$$

$$(\overline{w'q'})_0 = D_w C_H |V_1| (q_0 - q_1), \tag{2.4}$$

where V, u, v, w, θ, and q are the horizontal velocity vector; zonal, meridional, and vertical wind components; potential temperature; and specific humidity, respectively. The subscripts 0, 1 refer to values at the surface and at the lowest model level, respectively. Note that $\rho_1(\overline{w'u'})_0$ and $\rho_1(\overline{w'v'})_0$ are the surface stresses (ρ is density), while $c_p\rho_1(\overline{w'\theta'})_0$ and $L\rho_1(\overline{w'q'})_0$ are the sensible and latent heat fluxes, respectively.

Recognizing that $u_0 = v_0 = 0$, (2.1)–(2.3) have identical forms. The additional factor, D_w, in (2.4) represents the availability of water at the surface, and q_0 is defined as the saturation value of q at temperature θ_0. For the moment, D_w is specified over land as a geographically varying but time-independent value based on surface type data (similar as in CCM1). However, in future studies more refined land-surface schemes (e.g., Dickinson 1984; Pan 1990; Beljaars and Holtslag 1991) will be considered. Over sea, $D_w = 1$.

Following Louis et al. (1982) and Holtslag and Beljaars (1989), the two surface-layer exchange coefficients used in (2.1)–(2.4) are defined as

$$C_M = C_N f_M(\mathrm{Ri}_0), \tag{2.5}$$

$$C_H = C_N f_H(\mathrm{Ri}_0). \tag{2.6}$$

The neutral exchange coefficient is

$$C_N = \frac{k^2}{\ln((z_1 + z_{0M})/z_{0M}) \ln((z_1 + z_{0M})/z_{0M})}, \tag{2.7}$$

where $k = 0.4$ is the von Kármán constant, z_1 is the height of the lowest model level, and z_{0M} is the roughness length for momentum. Here, we have assumed that the roughness lengths for momentum, heat, and constituents are the same, which is not generally true (see Beljaars and Holtslag 1991). In CCM2, the roughness length over land varies geographically based on surface-type data (from 0.04 m over tundra, to 2 m over tropical rain forest), while over ocean $z_{0M} = 10^{-4}$ m.

The surface-layer *bulk* Richardson number in (2.5) and (2.6) is defined as

$$\mathrm{Ri}_0 = \frac{g z_1 (\theta_{v1} - \theta_{v0})}{\theta_1 |V_1|^2}, \tag{2.8}$$

where g is the acceleration of gravity, θ_{v1} and θ_{v0} are the virtual potential temperatures, and $|V_1|^2 \geq 1$. Under unstable conditions ($\mathrm{Ri}_0 < 0$), the functions that modify the neutral-exchange coefficient are taken from Louis et al. (1982):

$$f_M(\mathrm{Ri}_0) = 1 - \frac{10\,\mathrm{Ri}_0}{1 + 75C_N\{[(z_1 + z_{0M})/z_{0M})]\,\mathrm{Ri}_0|\}^{1/2}}, \tag{2.9}$$

$$f_H(\mathrm{Ri}_0) = 1 - \frac{15\,\mathrm{Ri}_0}{1 + 75C_N\{[(z_1 + z_{0M})/z_{0M}]|\mathrm{Ri}_0|\}^{1/2}}. \tag{2.10}$$

Under stable conditions ($\mathrm{Ri}_0 \geq 0$), the functions that modify the neutral-exchange coefficient are taken from Holtslag and Beljaars (1989):

$$f_M(\mathrm{Ri}_0) = f_H(\mathrm{Ri}_0) = \frac{1}{1 + 10\,\mathrm{Ri}_0(1 + 8\,\mathrm{Ri}_0)}. \tag{2.11}$$

The above forms for f_M and f_H are reasonable fits to available observations in the surface layer (see Holtslag and Beljaars 1989).

c. *Experiments*

A decadal integration of a test version of CCM2 was used as the starting point for the two experiments discussed here. The results presented below were obtained from two 60-day integrations of the model, beginning on 2 June of the seventh year of the decadal integration. In the first experiment, the ABL scheme was updated slightly (to that described below) from the scheme used in the decadal integration. In the second experiment, the ABL scheme was replaced by the local-K scheme. In all of the above experiments, the dry-adiabatic procedure was not used (except in the top three model layers). An additional pair of experiments was performed in which the dry-adiabatic adjustment was applied in all model layers. Results from the latter experiments will be mentioned below.

The results shown below are 31-day averages for July. The land-surface temperatures in the second (local-K) experiment are probably not yet in equilibrium, however, we will concentrate on results over ocean points.

The observations, used to compare against the model results, were obtained by taking the monthly averages of daily radiosonde reports of temperature and dewpoint depression from U.S. Control Sources. Dewpoint depressions were converted to specific humidities prior to averaging. The profiles show the July mean averaged over all available years (from 15 to >40 years depending on the station) and the standard deviation (interannual variability) of the monthly means. Comparison data from the model is taken by averaging all grid points within ±3° of the station.

3. The vertical-diffusion schemes

a. *Local diffusion scheme*

Turbulent mixing in global atmospheric models is usually treated by a first-order local diffusion approach, in which the subgrid-scale turbulent, vertical kinematic flux of a quantity is taken proportional to the local gradient of the transported quantity. This reads as

$$\overline{w'C'} = -K_c \frac{\partial C}{\partial z}, \tag{3.1}$$

where $C \in (q, \theta, u, v)$. The quantity K_c is an "eddy diffusivity" for C, which is typically taken as a function of a length scale l_c and local vertical gradients of wind and virtual potential temperature:

$$K_c = l_c^2 S F_c(\mathrm{Ri}). \tag{3.2}$$

Here, S is the local shear, defined by

$$S = \left|\frac{\partial V}{\partial z}\right|, \tag{3.3}$$

and l_c is given by

$$\frac{1}{l_c} = \frac{1}{kz} + \frac{1}{\lambda_c}, \tag{3.4}$$

where again k is the von Kármán constant and λ_c is the so-called asymptotic length scale. Furthermore, $F_c(\mathrm{Ri})$ denotes a functional dependence of K_c on the *gradient* Richardson number:

$$\mathrm{Ri} = \frac{g}{\theta_v}\frac{\partial\theta_v/\partial z}{S^2}, \tag{3.5}$$

where θ_v is the virtual potential temperature.

It is noted that both λ_c and $F_c(\mathrm{Ri})$ have to be specified, and that their formulation is rather empirical. Consequently, there have been a large number of papers dealing with the formulation of these quantities (e.g., Blackadar 1962; Mellor and Yamada 1974; Louis et al. 1982). In CCM1 (Williamson et al. 1987), l_c = 30 m was specified, which is thought to be representative for the free atmosphere. Louis et al. (1982) distinguish the asymptotic length scales for heat and momentum to be 450 and 150 m, respectively. However, in previous studies, a value of 300 m has been used for both heat and momentum. This value seems to be typical for the ABL but is probably too large for the free atmosphere.

For the present implementation of the local diffusion scheme, a simple approach was taken, choosing λ_c = 300 m for $z \leq 1$ km. In section 5 we show that with the latter value for λ_c, the local scheme can produce reasonable magnitudes for the eddy diffusivity in the boundary layer. For greater heights a smooth interpolation to the free atmospheric value of 30 m is used, according to

$$\lambda_c = 30 + 270\exp(1 - z/1000), \tag{3.6}$$

resulting in $\lambda_c = 35$ m at $z = 5$ km and $\lambda_c = 30$ m at $z = 10$ km. Since the actual length scale l_c depends on both λ_c and on z, according to (3.4), l_c increases with height to a maximum of 290 m near $z = 1$ km, and then decreases gradually above.

In our present implementation of the local diffusion approach, we specify the same stability functions F_c for all C for simplicity. For unstable conditions (Ri < 0) the following is chosen:

$$F_c(\mathrm{Ri}) = (1 - 18\ \mathrm{Ri})^{1/2} \qquad (3.7)$$

as in CCM1 (Williamson et al. 1987), and for stable conditions (Ri > 0), (2.11) is used, with Ri_0 replaced by Ri. This means that in this scheme no distinction is made between vertical diffusion of heat, scalars, and momentum above the surface layer. Note that the magnitude of the surface *bulk* Richardson number Ri_0 is generally different from that of the *gradient* Richardson number Ri just above the surface layer.

b. *The nonlocal ABL scheme*

As summarized above, in a local diffusion approach the flux of a quantity is proportional to the local gradient of that quantity [see Eq. (3.1)], and the eddy diffusivity depends typically on local gradients of mean wind and mean virtual temperature [see Eq. (3.2)]. These are reasonable assumptions when the length scale of the largest transporting turbulent eddies is smaller than the size of the domain over which the turbulence extends. This applies in the ABL typically for neutral and stable conditions only. For unstable and convective conditions, however, the largest transporting eddies may have a similar size as the boundary-layer height itself and, in particular, the heat flux can be counter to the local temperature gradient (Deardorff 1972; Holtslag and Moeng 1991; Stull 1991).

To illustrate the transports in a dry convective boundary layer, typical (virtual) potential temperature and specific humidity profiles for such a boundary layer have been given in Fig. 2. Also the heat and specific humidity fluxes are shown. For specific humidity, its flux is typically down the local gradient. This also applies for potential temperature in the indicated transport regions 1 and 3, but not for region 2. In the latter region, the temperature profile is typically adiabatic and even subadiabatic higher up, while at the same time, the heat flux remains upward. The upward heat flux arises from nonlocal transport by convective parcels, which initiate near the surface. As long as the virtual potential temperature of rising parcels is larger than the environment, the parcel will rise. In fact, the height of a convective turbulent boundary layer (with negligible winds) extends to the height where parcels intersect with the environmental temperature profile (Holzworth 1964).

Due to the rising parcels ("large-eddy motion") in the convective boundary layer, the turbulent transport

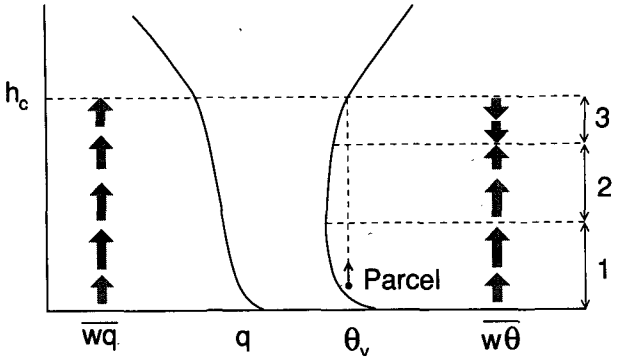

FIG. 2. Typical vertical profiles for (virtual) potential temperature Θ_v and specific humidity q for a dry convective boundary layer [modified after Stull (1991)]. The arrows to the left illustrate the specific humidity flux $\overline{wq}$, and the arrows to the right, the heat flux $\overline{w\theta}$. Also, an uprising parcel is indicated up to its intersection height h_c. The three regions are discussed in the text.

has a strong nonlocal character, and local diffusion by itself is not sufficient. Holtslag and Moeng (1991) discuss the nonlocal transport in a convective boundary layer. By simplifying the heat and scalar flux budget equations, they show that the flux of any scalar C can be described with

$$\overline{w'C'} = -K_c\left(\frac{\partial C}{\partial z} - \gamma_c\right). \qquad (3.8)$$

Here, K_c is an eddy diffusivity for the quantity of interest, $\partial C/\partial z$ is the local gradient for C, and γ_c reflects the nonlocal transport due to dry convection. Although despite of γ_c, Eq. (3.8) may look rather similar to (3.1), the formulation of the eddy diffusivity depends on characteristic, *bulk* properties of the ABL (see below) rather than local properties as in (3.2).

Equation (3.8) applies to potential temperature, water vapor, and other passive scalars. For temperature, the nonlocal transport term γ_θ is traditionally called the countergradient term (e.g., Deardorff 1972), because of its acting against the local gradient for $\partial\Theta/\partial z > 0$ (as in region 2 of Fig. 2). The nonlocal transport by convection also affects the transport by scalars such as specific humidity. For specific humidity, however, typically $\partial C/\partial z < 0$, and the nonlocal transport effect by γ_c works in the same direction as the local transfer (Fig. 2). This may explain why the specific humidity does not show a "countergradient" effect (Mahrt 1976). Note that even for $\partial C/\partial z = 0$, a finite flux will remain. Because of its physical background and its ability to describe the nonlocal transports in a convective boundary layer, we will refer to Eq. (3.8) as a *nonlocal* diffusion approach.

So far no nonlocal transport term has been derived for the wind components, so the format of (3.1) is retained for simplicity. Moreover, for stable and neutral conditions, the nonlocal transport term is not relevant for any of the quantities. The eddy diffusivity formu-

lation, however, is modified to be consistent with the one for unstable and convective conditions.

In the present application of the nonlocal diffusion scheme, the eddy diffusivity is given as (Troen and Mahrt 1986; Holtslag et al. 1990)

$$K_c = kw_t z\left(1 - \frac{z}{h}\right)^2, \tag{3.9}$$

where w_t is a characteristic turbulent velocity scale and h is the boundary-layer height. Equation (3.9) is applied for heat, water vapor, and passive scalars. The eddy diffusivity of momentum, K_m, is also defined as (3.9) but with w_t replaced by another velocity scale w_m. With proper formulation of w_t (or w_m), and h, it can be shown that Eq. (3.9) behaves well from very stable to very unstable conditions in horizontally homogeneous and quasi-stationary conditions. In fact, the turbulent velocity scale depends on height and stability (see the review by Holtslag and Nieuwstadt 1986). For unstable conditions, w_t and w_m are proportional to the so-called convective velocity scale w_*, while for neutral and stable conditions, w_t and w_m are proportional to the friction velocity u_*. A summary of the velocity scales is given in appendix A. Note that there is some empirism in the formulation of the velocity scales, due to their dependence on the empirical similarity functions. As discussed in section 3a, however, the local scheme also utilizes empirical quantities.

In general, the eddy diffusivity in (3.8) may depend on the transported scalar. Then the entrainment flux near the top of the ABL is relevant, in addition to the surface flux (Holtslag and Moeng 1991). Since consistent formulation of the entrainment flux within the nonlocal diffusion approach has not been solved in detail at the moment, we also used (3.9) for specific humidity. Moreover, we hesitated to introduce too much complexity in the scheme at once. Therefore, the present application of the nonlocal scheme can only be seen as an intermediate step to future improvements.

Note that Eq. (3.9) is very similar to the one proposed by Brost and Wyngaard (1978) for the stable boundary layer. The cubic shape of (3.9) is consistent with the eddy-diffusivity profile originally proposed by O'Brien (1970), which he derived on the basis of the physical requirements that the profile and its first derivative be continuous with height and match to surface layer similarity.

The nonlocal transport term in (3.8), γ_c, represents nonlocal influences on the mixing by turbulence. As such, this term is small in stable conditions, and is, therefore, neglected in these conditions. For unstable conditions, however, most transport of heat and moisture is done by turbulent eddies with sizes on the order of the depth h of the ABL. In such cases, a formulation for γ_c, consistent with the eddy formulation of (3.8), is given by

$$\gamma_c = a\frac{w_*(\overline{w'C'})_0}{w_m^2 h}, \tag{3.10}$$

where a is a constant (see appendix A) and $(\overline{w'C'})_0$ is the surface flux (in kinematic units) of the transported scalar, which may be water vapor or potential temperature. So far, no nonlocal term applies to momentum, as noted above. The form of (3.10) is similar to the one obtained in Holtslag and Moeng (1991). The nonlocal correction term vanishes under neutral conditions, for which $w_* = 0$. The latter property is desirable and was not apparent in the original form for γ_c by Troen and Mahrt (1986).

The formulations of the eddy-diffusivity and the nonlocal correction terms are dependent on the boundary-layer height h. We follow Troen and Mahrt (1986) and determine h iteratively by using

$$h = \frac{\mathrm{Ri}_{cr}[u(h)^2 + v(h)^2]}{(g/\theta_s)(\theta_v(h) - \theta_s)}, \tag{3.11}$$

where Ri_{cr} is a critical bulk Richardson number for the ABL, $u(h)$ and $v(h)$ are the horizontal velocity components at h, g/θ_s is the buoyancy parameter, $\theta_v(h)$ is the virtual temperature at h, and θ_s is an appropriate temperature of air near the surface. The value of the critical bulk Richardson number, Ri_{cr} in (3.11), depends generally on the vertical resolution of the model. For our (still rather crude) vertical model resolution, we use $\mathrm{Ri}_{cr} = 0.5$.

Following Troen and Mahrt (1986), θ_s for unstable conditions is given by

$$\theta_s = \theta_v(z_s) + b\frac{(\overline{w'\theta'_v})_0}{w_m}, \tag{3.12}$$

where b is a constant (see appendix A), $(\overline{w'\theta'_v})_0$ is the virtual heat flux at the surface, and unstable conditions are determined by $(\overline{w'\theta'_v})_0 > 0$. In (3.12), $\theta_v(z_s)$ is a virtual temperature in the atmospheric surface layer (say at a height of 10 m). The second term on the rhs of (3.12) represents a temperature excess, which is a measure of the strength of convective thermals in the lower part of the ABL. This value, and a similar one for moisture, is also used by the convection scheme (Hack 1993) to provide a direct coupling between the surface fluxes and the convection parametrization.

The above-described determination of h for unstable conditions, incorporates both the effects of mean wind shear and convection. Note that in the limit of free convection, Eq. (3.11) provides that $\theta_v(h) = \theta_s$, which is consistent with the dry-parcel intersection method illustrated in Fig. 2. For stable conditions $(\overline{w'\theta'})_0 < 0$, and we apply

$$\theta_s = \theta_v(z_s), \tag{3.13}$$

with $z_s = 10$ m. The latter virtual temperature is calculated from the temperature and moisture of the first model level and of the surface by applying the procedure in Geleyn (1988).

On the basis of (3.11) the boundary-layer height h can be determined by iteration for all stability conditions when the surface fluxes and the profiles of θ_v, u,

and v are known. The computation starts by calculating the bulk Richardson number Ri between the level of θ_s and subsequent higher levels of the model. Once Ri exceeds the critical value, the value of h is derived by linear interpolation between the level with Ri > Ri_{cr}, and the level below.

Using the calculated value for h and the surface fluxes, we calculate the velocity scales (appendix A), the eddy diffusivities with (3.9), and the nonlocal transport terms with (3.10) for each quantity of interest. Above the ABL, $\gamma_c = 0$, so (3.8) reduces to (3.1). Then K_c is given by (3.2), where we have $l_c = 30$ m. Near the top of the ABL we use the maximum of the values by (3.2) and (3.9), although (3.9) almost always gives the larger value in practice. Subsequently, the new profiles for θ, q, u and v are calculated with an implicit diffusion equation (appendix B).

4. Sample profiles and comparison with observations

In Fig. 1 we have shown the simulations with the two diffusion schemes within CCM2, in comparison with the observed vertical temperature and specific humidity profiles for Truk Island. Here, similar comparisons are presented for another tropical ocean point (San Juan), a subtropical ocean point (Azores), and a land point (W. Europe). Recall that over the oceans, the sea surface temperature is prescribed, and that the model results represent 31-day averages for July, while the observations are taken from at least 15 "July" months (see section 2c). So, some deviation of the model simulations with the mean observed values is to be expected.

Figure 3 shows the results for San Juan (18.3°N, 66.0°W). It is seen that the temperature profile in the lower atmosphere (up to 850 mb) is reasonably well represented with both diffusion schemes. The model simulations show deficiencies above the 800-mb level that are not directly related to the vertical-diffusion schemes, but to other model aspects. Below 800 mb the simulations with the two diffusion schemes are quite different (as in Fig. 1 for Truk Island). Note that the model simulation with the nonlocal diffusion scheme affects a much deeper layer than the simulation with the local diffusion scheme. The nonlocal simulation underscores the observed value at 1000 mb, while the local scheme underscores the 900-mb specific humidity observation. To illustrate the difference in the simulations with the two schemes, we studied the simulations with the two diffusion schemes with *instantaneous*

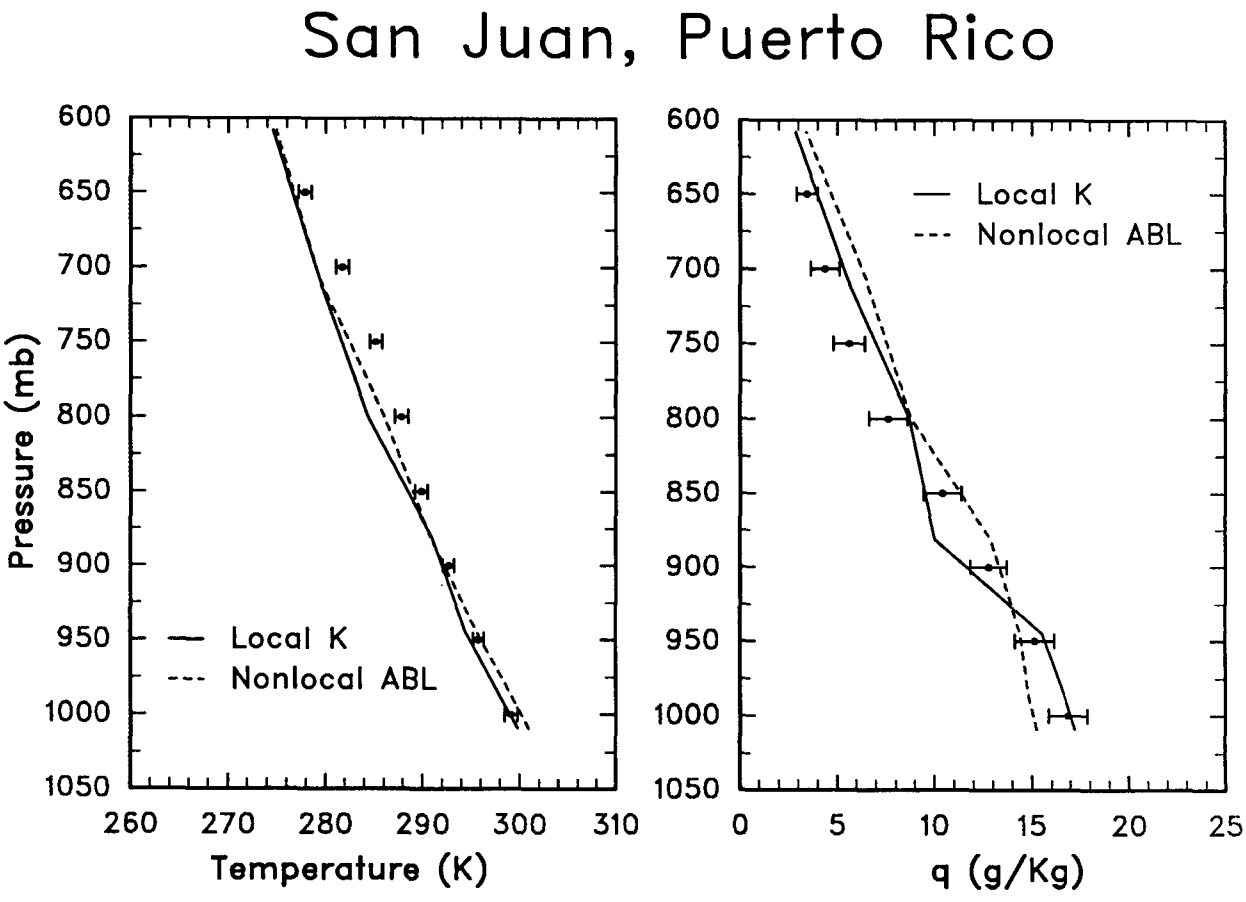

FIG. 3. As Fig. 1 but for San Juan, Puerto Rico (18.3°N, 66°W).

(not time averaged) model output for the mean profiles (e.g., u, v, θ, q) and surface forcing.

Figure 4 shows the instantaneous model output for the grid point near San Juan for a local time of 1600. The profiles of the mean profiles (upper panels) are obtained after 45 days of model integration with the nonlocal ABL scheme. As such they reflect typical afternoon conditions in the trade-wind region of the tropics. The boundary-layer height h is approximately 1400 m, and the surface stability is near-neutral, for example, $c_p\rho_1(\overline{w'\theta'})_{v0} \approx 5$ W m^{-2}. The surface fluxes are $c_p\rho_1(\overline{w'\theta'})_0 \approx -10$ W m^{-2}, $L\rho_1(\overline{w'q'})_0 \approx 180$ W m^{-2}, and $u_* \approx 0.26$ m s^{-1}. It is seen that near the top of the ABL, the actual specific humidity is near its saturation value, indicating low cloud development. The virtual temperature profile in the ABL is slightly stable, and the wind shear in the ABL is relatively small.

In the lower panels of Fig. 4, we have given the profiles for the eddy diffusivity for heat (K_H), the moisture flux ($\overline{w'q'}$), and the tendency due to the nonlocal vertical diffusion scheme ($(\partial q/\partial t)_{VD}$). It is seen that the eddy diffusivity amounts up to 30 m^2 s^{-1} and that the

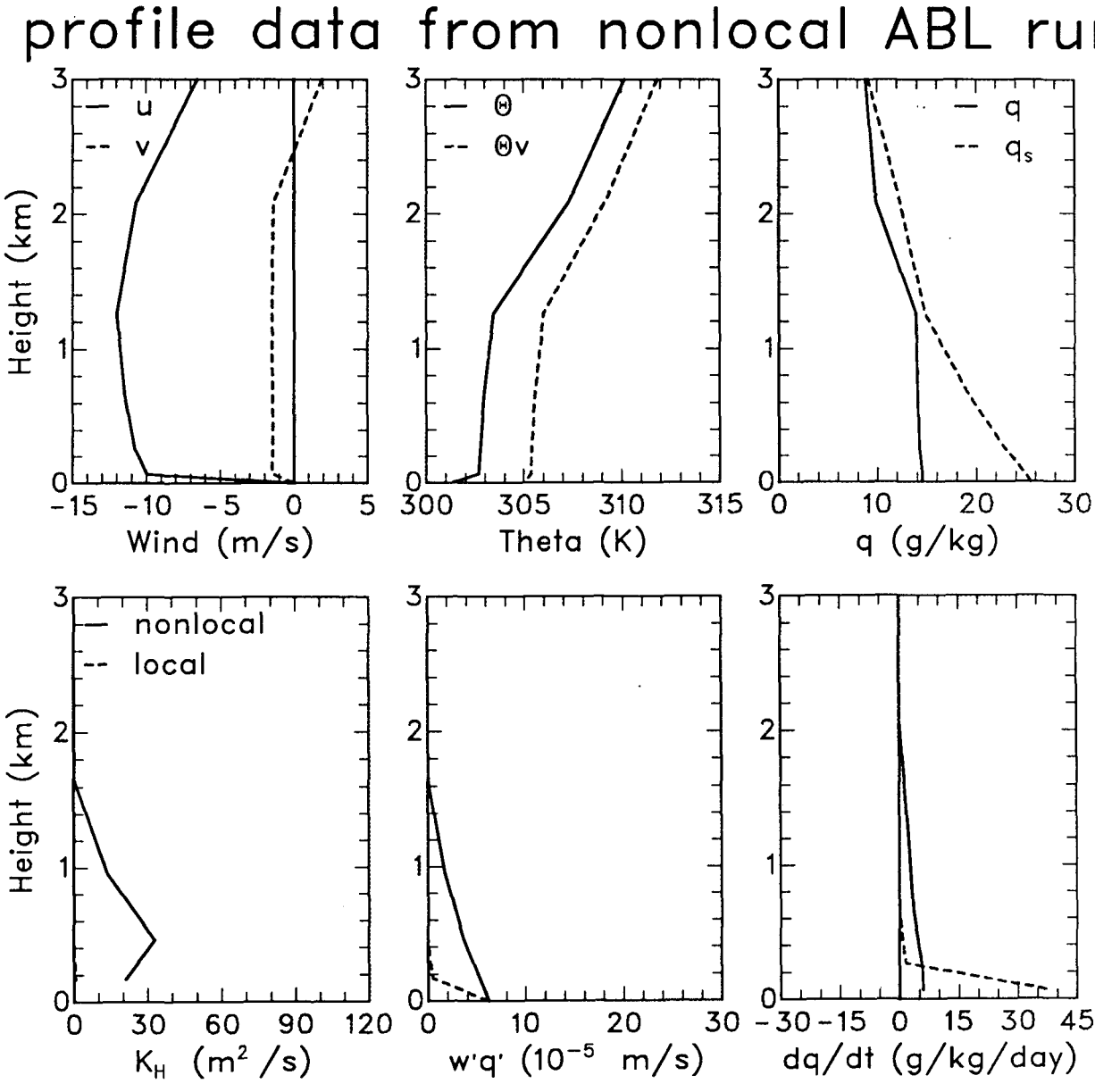

FIG. 4. Instantaneous profile data from a run with the nonlocal ABL scheme (upper panel) and the results (lower panel) for the eddy diffusivity, the specific humidity flux, and the specific humidity tendency using the nonlocal diffusion scheme (solid lines). Also, for comparison, the results of the local diffusion scheme are given in the lower panel (dashed lines), if the profiles of the upper panel are used as input. (The value of K_H with the local scheme is too small to be reproduced).

moisture flux is distributed across the whole ABL. Note that the moisture tendency affects a deeper layer than just the ABL, due to entrainment of dry air.

For *illustration purposes* we also show the outputs of the local diffusion scheme using the same mean profiles of the upper panel as input. Since, the virtual temperature gradient is stable, and the shear rather small, the local gradient Richardson number Ri is relatively large (Ri = 0.27 in the lower part of the ABL, increasing to Ri = 25 near z = 950 m). Consequently, the local diffusion scheme produces a very small value for the diffusivity (K_H = 0.39 m^2 s^{-1} in the lowest layer, almost two orders of magnitude smaller than with the nonlocal scheme for the same inputs), and the surface flux is redistributed in a rather thin part of the ABL.

Figure 5 shows the *instantaneous* profiles resulting from the 45-day model integration with the local scheme. Comparison of the profiles for u, v, θ, and q with those of Fig. 4 shows that the instantaneous profiles are quite different in the lower atmosphere. Figure 5 shows that the ABL has an unstable virtual temperature profile up to 600 m, and that the ABL height is about 700 m. The surface fluxes are now $c_p\rho_1(\overline{w'\theta'})_{v0} \approx 25$ W m^{-2}, $c_p\rho_1(\overline{w'\theta'})_0 \approx 12$ W m^{-2},

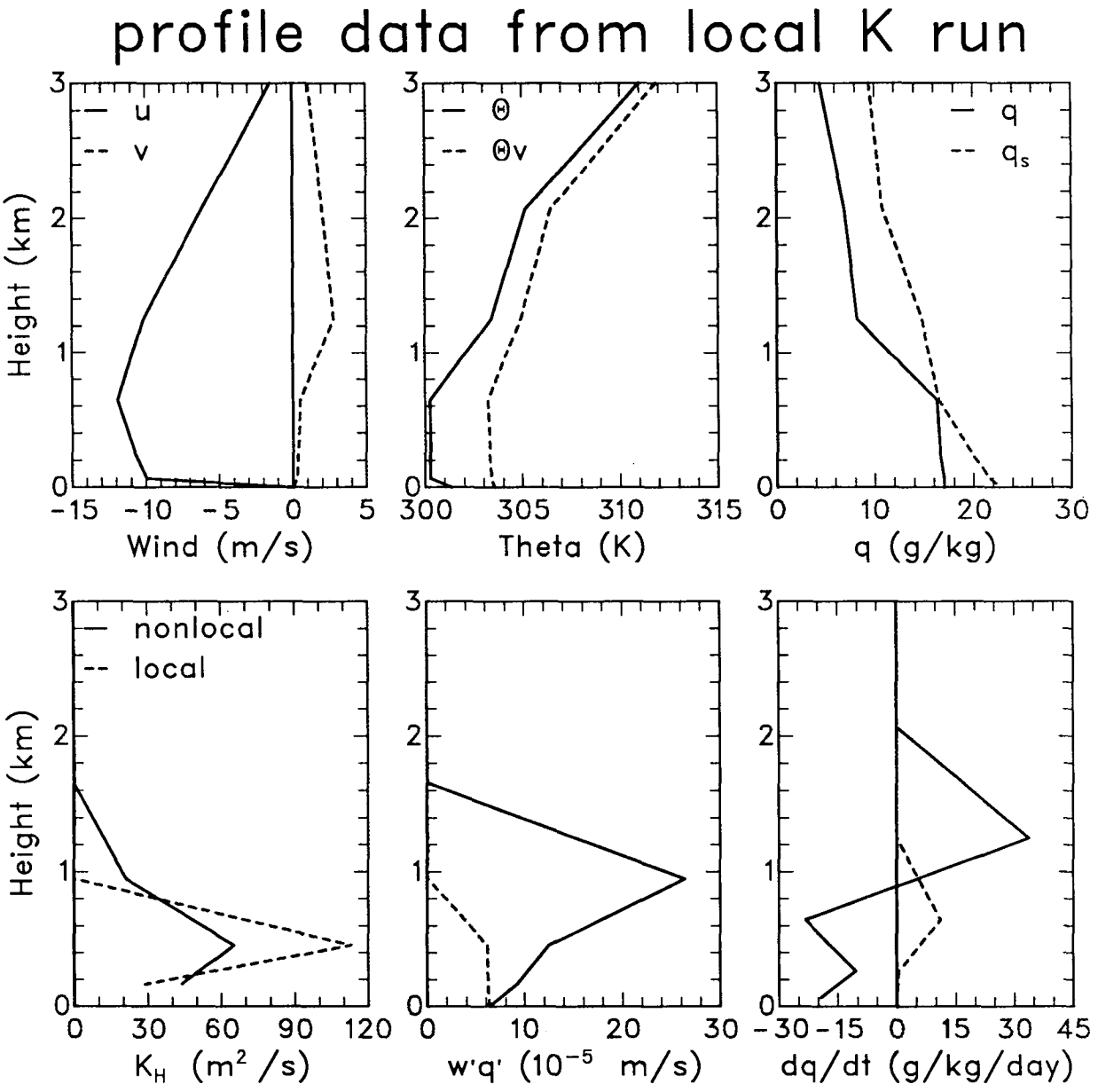

FIG. 5. Instantaneous profile data from a run with the local diffusion scheme (upper panel) and the results (lower panel) for the eddy diffusivity, the specific humidity flux, and the specific humidity tendency using the local diffusion scheme (dashed lines). Also for comparison the results of the nonlocal diffusion scheme are given in the lower panel (solid lines), if the profiles of the upper panel are used as input.

$L\rho_1(\overline{w'q'})_0 \approx 184$ W m^{-2}, and $u_* \approx 0.30$ m s^{-1}. Note that the surface sensible heat flux is now positive, resulting in a much larger surface virtual heat flux than with respect to Fig. 4. The evaporation into the atmosphere is about the same, while the surface stress is about 30% larger.

The lower panel of Fig. 5 shows the resulting profiles of the eddy diffusivity K_H, the moisture flux, and the moisture tendency of the local diffusion scheme. It is seen that the local scheme, with our choice of the asymptotic length scale (see section 3a), is capable of producing large values for K_H, but only by adjusting the virtual temperature profile. In a first-order local-diffusivity approach this is the only way to transport heat and moisture upwards. However, even in that case the height of the boundary layer is less than with the nonlocal approach and, consequently, the vertical transports of heat and moisture are affected. In the lower panels of Fig. 5, we have also illustrated the results obtained with the nonlocal scheme, using the profiles of the upper panel as input. The nonlocal scheme directly attempts to adjust the profiles and tries to do the mixing across a deeper layer.

Overall, the instantaneous profiles for temperature and specific humidity of Figs. 4 and 5 are consistent with the mean profiles of Fig. 3, although some internal model variability may be apparent. The comparison of the behavior of the two schemes in the previous examples, explains the difference in the simulated mean profiles of Fig. 3. The *instantaneous* differences in the ABL of potential temperature and specific humidity, amount up to 3 K and 3 g kg^{-1}, respectively. It is clear that this may have an important impact on the appearance of low clouds. In fact, Fig. 4 indicates low cloud formation near 1400 m, while Fig. 5 indicates low clouds near 600 m. The relatively low value of the specific humidity at 1000 mb in Fig. 3 may indicate that either the entrainment of dry air into the ABL is too big with the nonlocal scheme for this case, or that the interaction with the convection scheme is too strong. In future studies we will focus on these aspects in more detail.

Figure 6 shows the observed profiles for θ and q in comparison with the local and nonlocal simulations for the ocean grid point near the Azores (38.7°N, 27.1°W). It is seen that the temperature profile for the Azores is well represented with the nonlocal scheme. The vertical structure of the vertical humidity profile is also well represented, although the absolute values are slightly too large compared to the mean observed value. Again the local diffusion scheme shows its typical sharp decrease in moisture relatively close to the surface.

Figure 7 shows the results for the land point representative for western Europe (50.0°N, 5.0°E). It is seen that the temperatures simulated with both schemes match the observations near the surface but are too cool higher up. The simulation with the local scheme performs well for specific humidity, while the nonlocal scheme is too dry in the ABL. This is probably due to the fact that in the current surface parameterization, the surface moisture is not a variable but is prescribed and calibrated to the previous local diffusion scheme of CCM1 (see section 2b). We realize that the performance of the schemes over land is related to the parameterization of the surface energy budget, which is rather simple in the present study. For that reason we focused mostly on ocean points.

From the comparisons in Figs. 1, 3, 6, and 7, important differences in the simulations with the two diffusion schemes may be noted. We realize that these results also depend on the different interactions of the two diffusion schemes with other parts of the model. Since no attempt was made to calibrate the diffusion schemes to give the best possible simulations, the present comparisons can only serve as illustrations of their impact. It appears that for locations in which deep convection is important, the outputs of the runs with the two vertical-diffusion schemes are very similar (not shown here).

5. Global model diagnostics

a. *Vertical diffusion*

The impact of the ABL scheme on the global simulation is most conveniently summarized using zonally and time-averaged quantities. First, the mean diffusivities and the resulting temperature and specific humidity tendencies produced by the two simulations (Figs. 8–10) are examined, then the resulting changes in the temperature, specific humidity, and cloud amount (Fig. 11) are examined. Finally, results for the boundary-layer height are given in Fig. 12, which are obtained with the nonlocal scheme. All of the figures represent the July case (see section 2c).

The mean diffusivities (K_H) produced by the two schemes are similar in magnitude, although substantial differences are apparent in Fig. 8. Both schemes produce typical maximum diffusivities near 50 m^2 s^{-1} throughout the Southern Hemisphere, with the nonlocal diffusion scheme actually producing slightly larger mean values at higher levels. The peak at 50°S with the nonlocal scheme, is related to the location of the storm tracks in the Southern Hemisphere. Both diffusion schemes produce a deeper region of large diffusivity between 20° and 30°N, primarily associated with deep daytime mixing over subtropical land masses (the Sahara desert in particular). Note that the local-K scheme must maintain absolutely unstable conditions in the lower levels of the model in order to produce $K_H \sim 50$ m^2 s^{-1}.

The gross structure and magnitude of the T and q tendencies produced by the two schemes (Figs. 9 and 10) are similar, although significant differences are again apparent. The most obvious difference in the T tendencies is that the nonlocal ABL scheme produces cooling *above* the boundary layer in the tropics, through

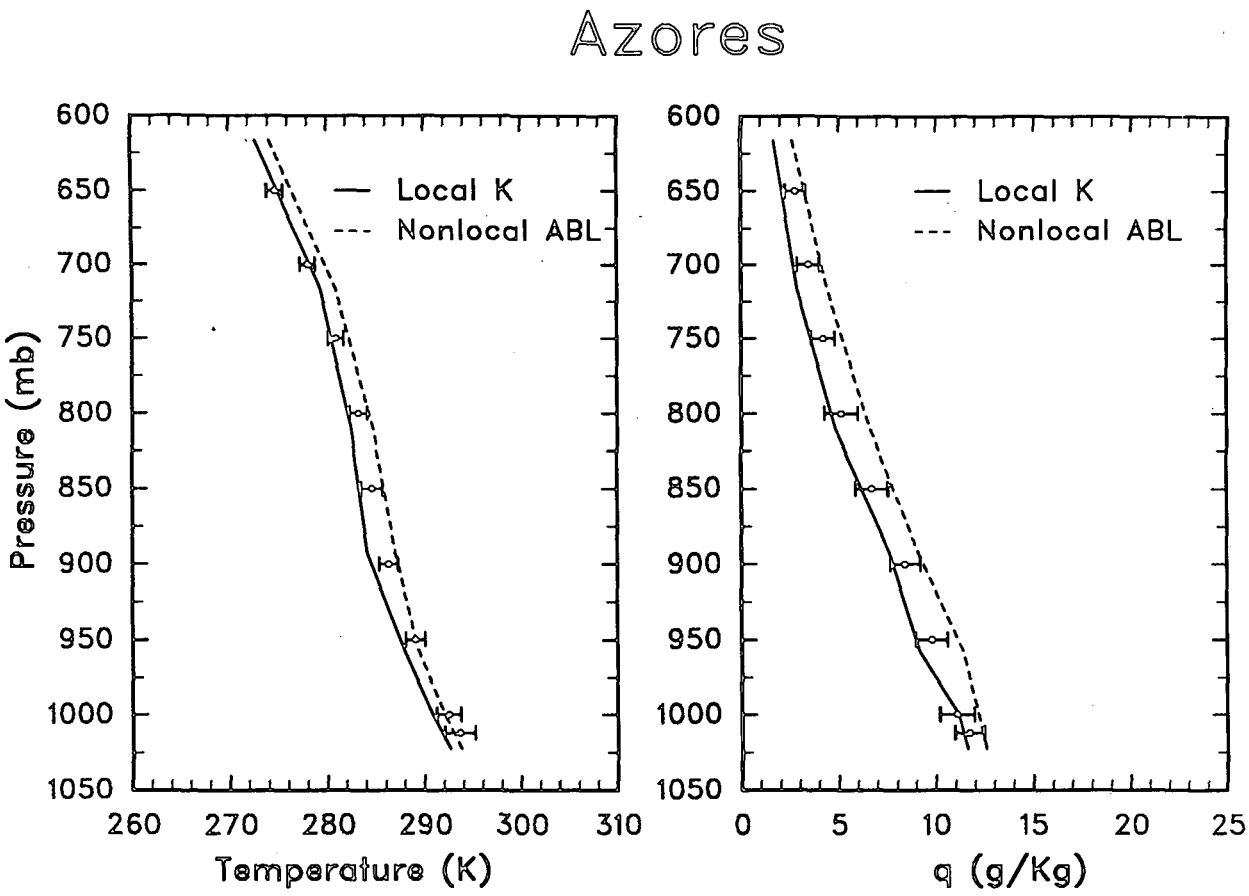

FIG. 6. As Fig. 1 but for the Azores (38.7°N, 27.1°W).

downward mixing of stably stratified air into the boundary layer (entrainment). This cooling is not found in the local diffusion scheme, because in the latter scheme entrainment is not represented.

The differences in the q tendency are more obvious than in the T tendency. The nonlocal ABL scheme carries the surface-water (latent heat) flux to higher levels, as seen in the profiles above. The region of large q tendency extends above 850 mb in the nonlocal ABL case and is confined below 850 mb in the local-K case. The deeper mixing of water by the nonlocal ABL makes the water more readily available to the convection parameterization. It should be noted that the tendency is essentially the flux divergence divided by the mass of the layer, and that the mass (thickness) of the layers increases rapidly with height in the boundary layer (see the model levels indicated in section 2a). The maximum tendencies are larger in the local-K case because the flux divergence is confined to a shallower region, not because the surface fluxes are larger.

The nonlocal scheme utilizes nonlocal transport effects for heat and moisture. From sensitivity studies with the model, we found that a factor-of-two variation in magnitude of the nonlocal transport terms has only a minor influence on the simulations. However, when the nonlocal transport terms are removed, there is a significant impact. By neglecting the nonlocal transport term, the magnitude of the boundary-layer height is reduced and, consequently, the diffusivities are smaller. This impacts on the entrainment of air into the ABL.

Finally, we studied the impact of dry-adiabatic adjustment in combination with either one of the diffusion schemes; the dry-adiabatic adjustment with the nonlocal ABL scheme makes very little difference in the diffusivities or in the T and q tendencies. However, including dry-adiabatic adjustment with the local-K scheme changes the above results dramatically. By eliminating unstable profiles, the adjustment procedure eliminates all large diffusivities and results in very large tendencies in the first model level. The surface fluxes of heat and water are deposited in the first model layer, with little diffusion to higher levels. If specific humidity is assumed to be well mixed following adjustment, then the dry adjustment replaces vertical diffusion as the principal vertical transport process for water in the lower layers of the model.

b. Effect on the simulation

The net effect of replacing the nonlocal ABL scheme with the local-K scheme is summarized in Fig. 11,

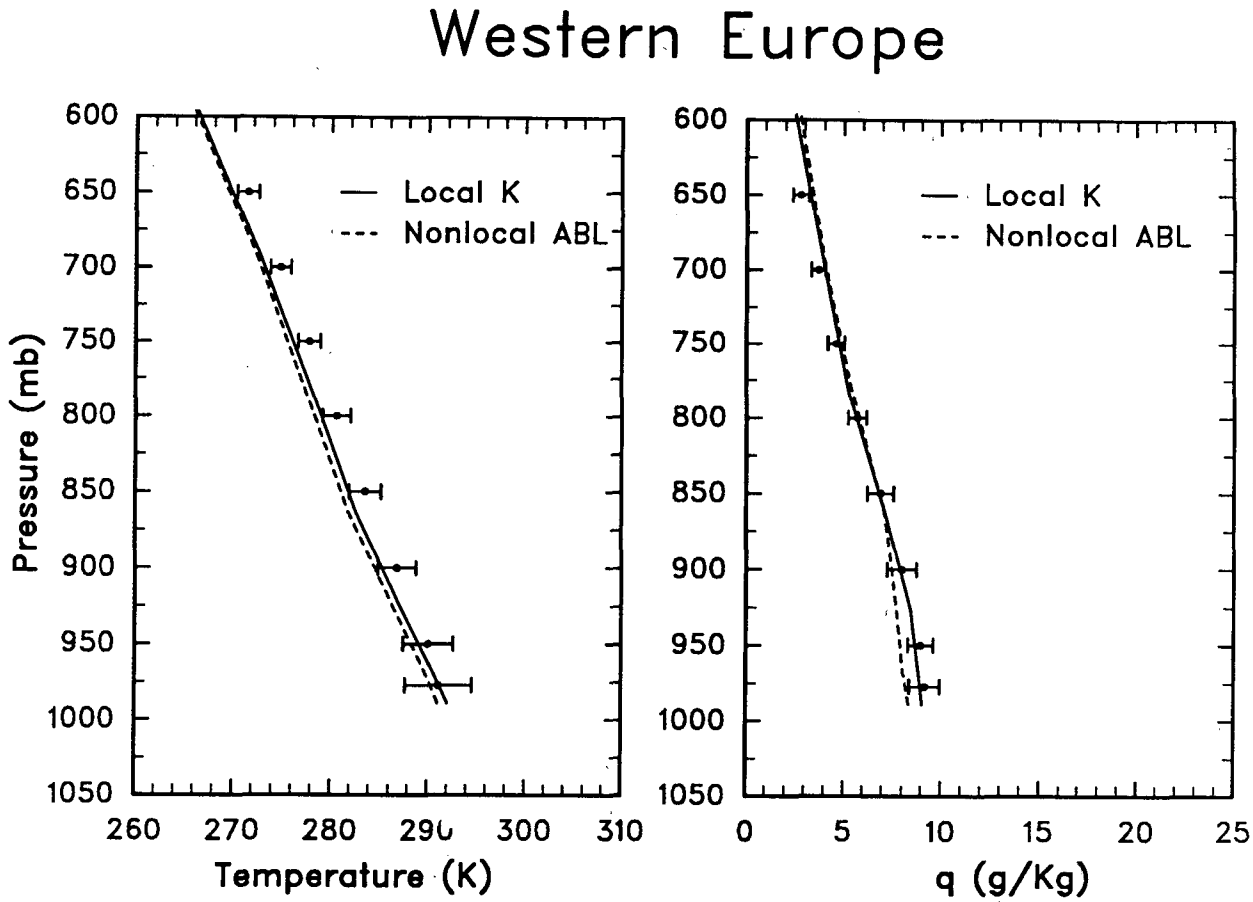

FIG. 7. As Fig. 1 but for a grid point in western Europe (50.0°N, 5.0°E).

which shows the *differences* in the zonal mean temperatures, specific humidities, and areal extent of cloudiness. The lower troposphere is warmer in the nonlocal ABL case throughout the tropics and middle latitudes. This change is almost certainly significant, although the experiments are too short for statistical testing. The specific humidity shows the difference anticipated from the individual profiles and the tenden-

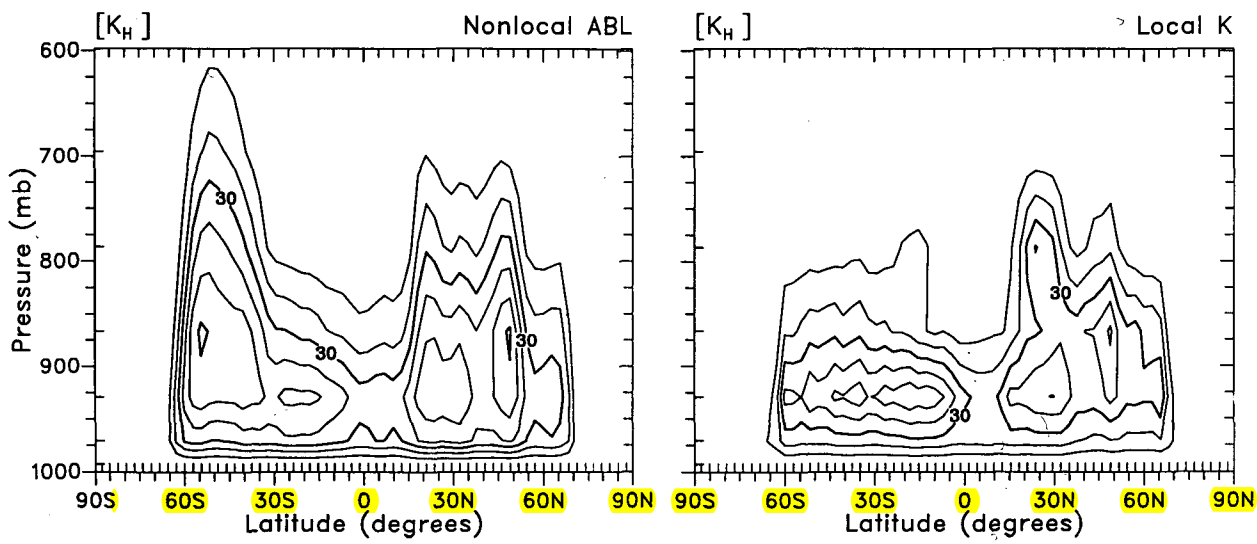

FIG. 8. Zonal mean July values for the eddy diffusivity calculated with the nonlocal (left panel) and local (right panel) diffusion schemes versus pressure. Contours are from 0 to 60 $m^2 s^{-1}$ with an interval of 10 $m^2 s^{-1}$ for the left panel and up to 50 $m^2 s^{-1}$ for the right panel.

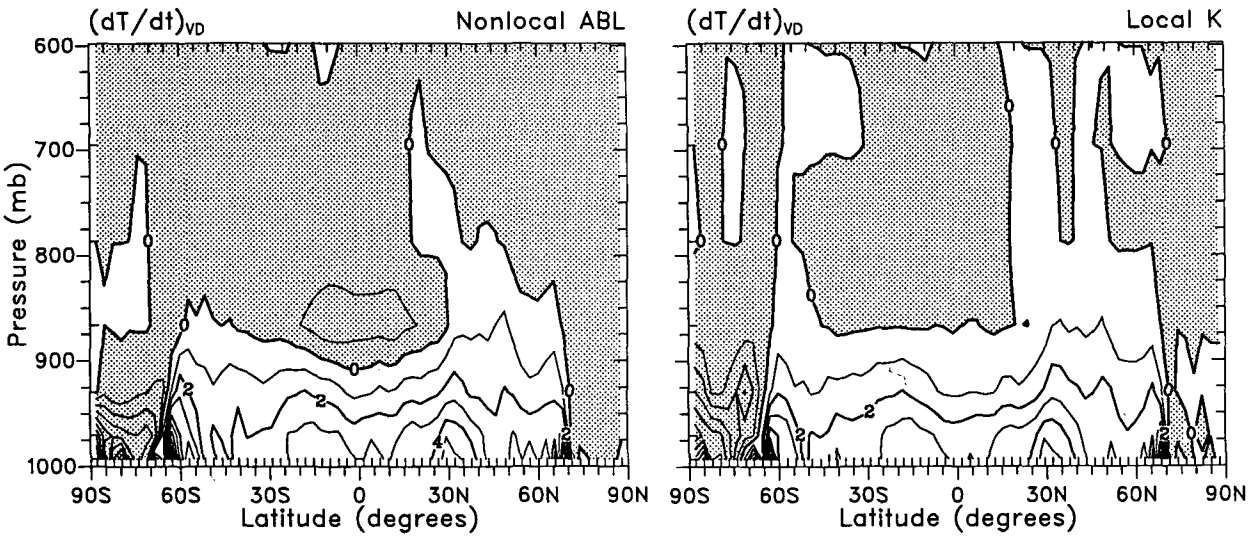

FIG. 9. As in Fig. 8 but for the temperature tendencies due to vertical diffusion. Contours are from −9 to 9 K s^{-1} with an interval of 1 K s^{-1} for the left panel and from −5 to 8 K s^{-1} for the right panel. The dotted area reflects negative values.

cies. The nonlocal ABL scheme dries the lowest model levels and moistens near 850 mb relative to the local-K scheme.

There are several important consequences for the rest of the model that follow from the upward shift in the water distribution between the nonlocal ABL and the local-K cases. There are direct impacts on both the convection and the clear-sky radiative processes. There is also a significant change in the distribution of low clouds. Although the net cloud amount below 700 mb is similar in both cases, the clouds are shifted upward in the nonlocal ABL case (Fig. 11). Very low clouds, which tend to form in the bottom two model levels with the local-K scheme, are virtually eliminated by the nonlocal ABL scheme, resulting in a more realistic cloud distribution.

c. *Boundary-layer height*

In the nonlocal ABL scheme the boundary-layer height h is calculated explicitly. Figure 12 shows the July-mean value for h and its diurnal range. The diurnal range of h was determined from the daily average maximum and minimum values of h based on hourly data. The minimum contour in the upper panel in Fig. 12 is 500 m, but $h < 200$ m over most of Antarctica and $h < 100$ m over a substantial region near the South Pole. The largest mean values of h are near 2 km in the Southern Hemisphere storm tracks, while $h \sim 1$ km over the tropical and midlatitude oceans. The mean boundary-layer heights are generally small (<1000 m) over the Southern Hemisphere continents, and even an island, such as Madagascar, can easily be located

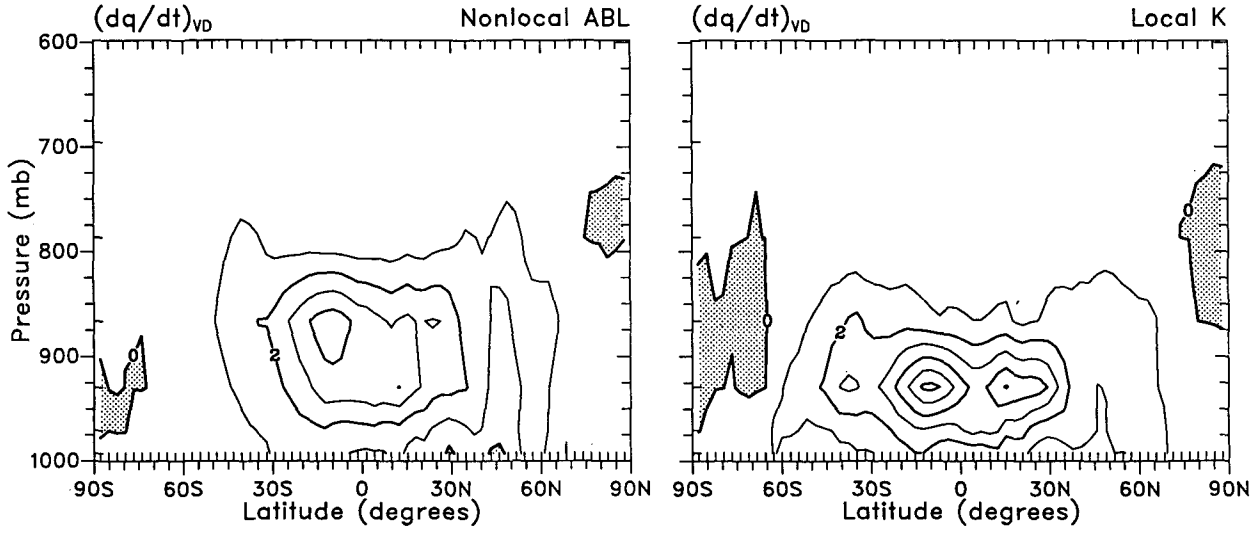

FIG. 10. As in Fig. 8 but for the specific-humidity tendencies due to vertical diffusion. Contours are from 0 to 4 g (kg s^{-1}), with an interval of 1 g (kg s^{-1}) for the left panel and up to 6 g (kg s^{-1}) for the right panel. The dotted area reflects negative values.

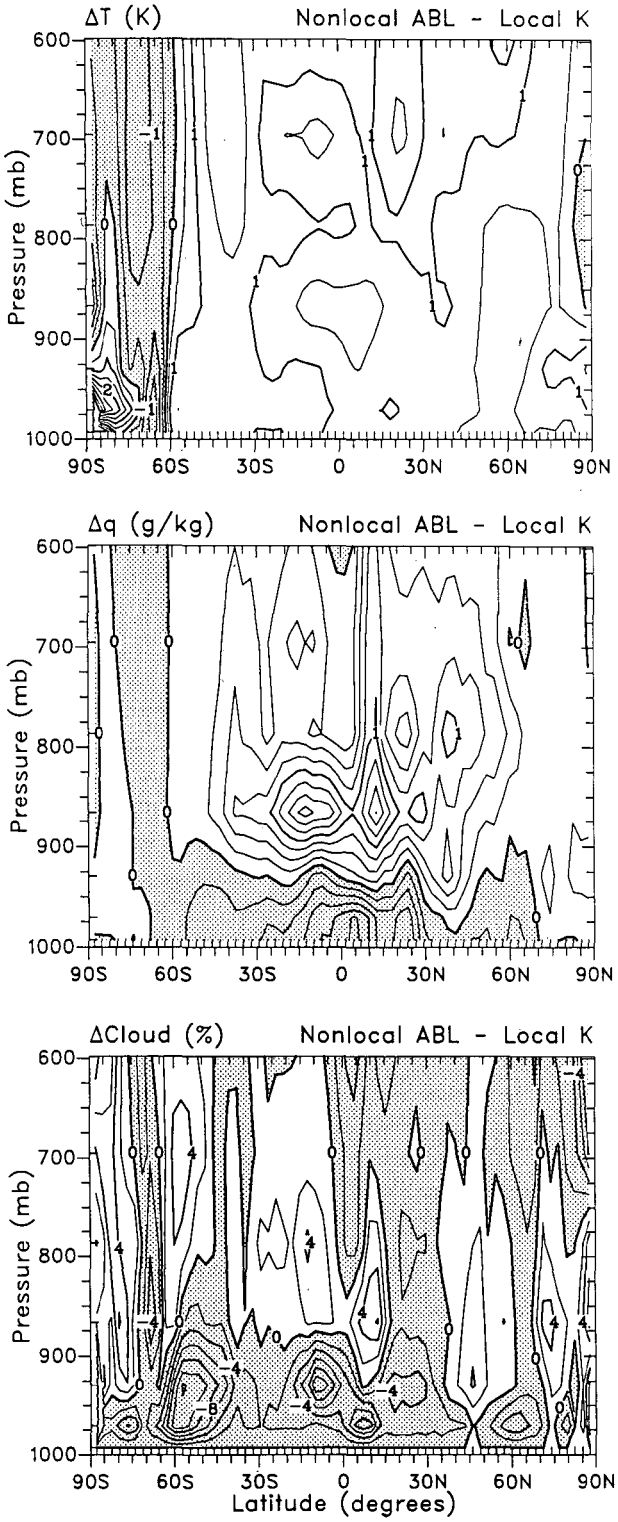

FIG. 11. Zonal mean differences between simulations with the nonlocal and local diffusion schemes versus pressure for July. Upper panel is for the temperature difference for which contours are plotted from −2.5 K to 5.5 K, with an interval of 0.5 K; middle panel is for the specific-humidity difference for which contours are given from −1.25 g kg^{-1} to 1.75 g kg^{-1}, with an interval of 0.25 g kg^{-1}; lower panel is for cloud fraction for which contours are given from −14% to 8%, with an interval of 2%. Dotted area reflects negative values.

in Fig. 12 by its smaller mean values for h (but larger diurnal ranges). Northern Hemisphere land points generally have mean values for $h > 1$ km. However, the typical diurnal range of h over land points is so large that the mean value may not be particularly useful.

The diurnal variation of h arises primarily from its dependence on the surface temperature and the surface fluxes of sensible and latent heat, through (3.11) and (3.12). The variation of these quantities is small over oceans (in fact, the surface temperature is fixed), so the diurnal range of h is also small over oceans ($\ll$500 m). In contrast, all land points have diurnal ranges of $h >$ 500 m except over Antarctica and the small snow-covered areas at high latitude in North America and Asia. As expected, the diurnal range of h is largest over the Sahara desert, where it approaches 4 km. In this region the boundary-layer depth collapses to <100 m at night and increases rapidly after sunrise to ~4 km. A similar diurnal cycle is found over most of the summer continental regions, although the nighttime minimum and daytime maximum are typically not as extreme as in the Sahara.

6. Summary and conclusions

In this paper we have studied the impact of a local and a nonlocal scheme for vertical diffusion in the atmospheric boundary layer (ABL) within the context of the NCAR Community Climate Model, version 2 (CCM2). The local diffusion scheme uses an eddy diffusivity determined independently at each point in the vertical based on local vertical gradients of wind and virtual potential temperature. The nonlocal scheme determines an eddy-diffusivity profile based on a diagnosed boundary-layer height and a turbulent velocity scale. It also incorporates nonlocal (vertical) transport effects for heat and moisture, and a direct coupling to the parameterization of deep and shallow convection (see section 3).

The outputs of the local and nonlocal diffusion schemes have been compared for sample profiles and with radiosonde observations for a number of locations. The vertical structure of the temperature and humidity profiles, simulated with the local and nonlocal diffusion schemes, shows important differences. We realize that these results depend on the different interactions of the two diffusion schemes with other parts of the model. Since no attempt was made to calibrate the diffusion schemes to give the best possible simulations, the present comparisons can only serve as illustrations of the impact. It also appears that for locations in which deep convection is important, the outputs of the runs with the two vertical-diffusion schemes are very similar.

Nevertheless, over tropical oceans we showed that the simulation with the nonlocal scheme is generally more realistic. In this region, the local scheme does not transport water away from the surface as rapidly or deeply as does the nonlocal scheme. In fact, the local

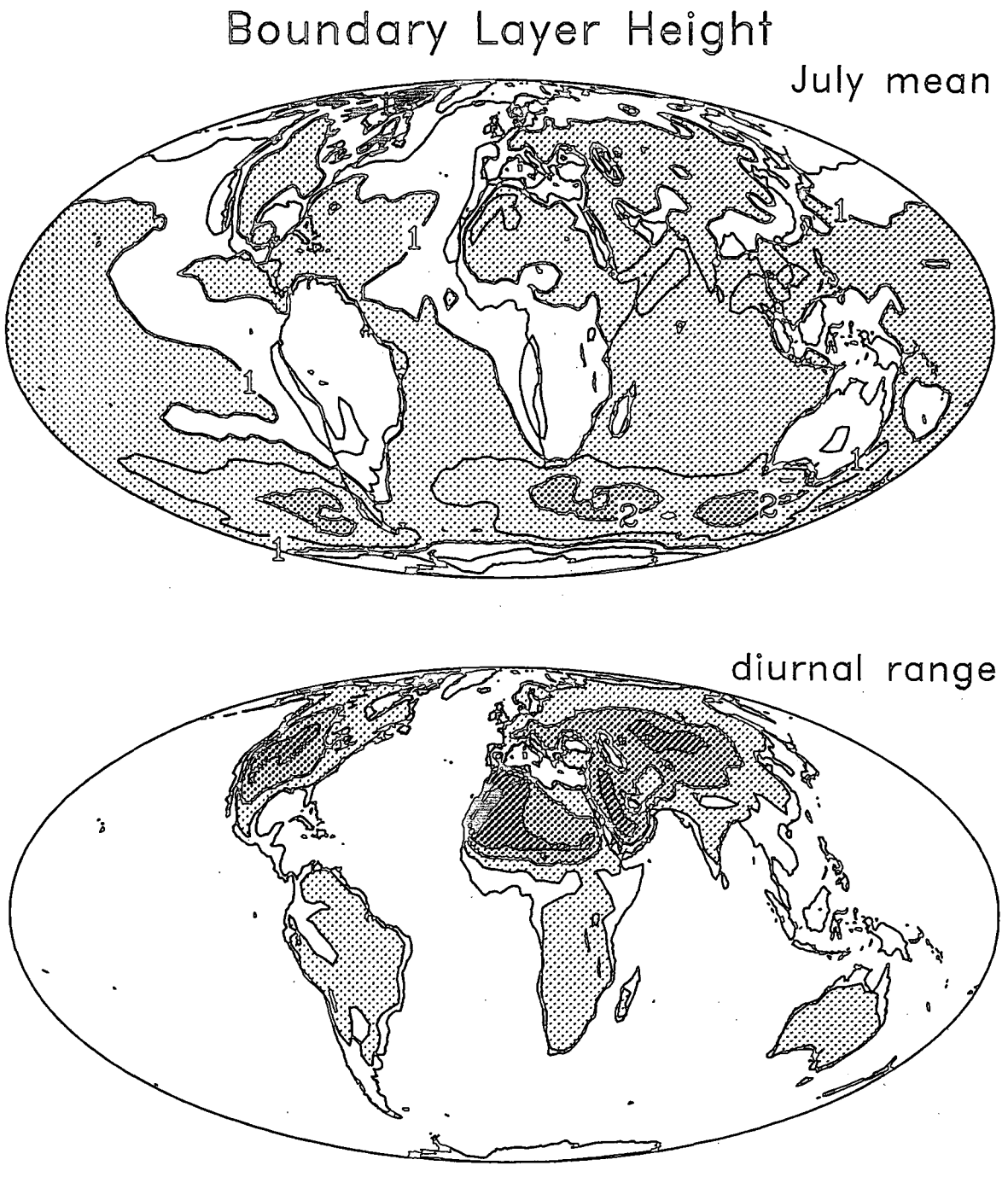

FIG. 12. July mean values of boundary-layer height (upper panel) and diurnal range (lower panel). Contours are from 0.5 km to 4 km, with an interval of 0.50 km for the upper panel. Shading increases with the represented value. In the lower panel, the white regions refer to cases with a diurnal range less than 1 km, light dotted areas refer to a range of 1 to 2 km, and heavier dotted areas refer to cases with a diurnal range larger than 2 km up to more than 4 km over the Sahara desert.

scheme must maintain an absolutely unstable profile across the depth of the boundary layer in order to produce significant transport of water. In addition, the upward transport of heat can only occur for absolutely unstable profiles in a local diffusion approach. The nonlocal scheme responds directly to upward surface fluxes and can produce significant transports for both water and heat, while maintaining slightly subadiatic temperature profiles as typically observed in the upper part of the boundary layer. It is also noted that the nonlocal scheme is more robust to numerical oscillations (Beljaars 1991).

The differences due to the two diffusion schemes in the low-level *mean* temperature and specific humidity

are typically in the order of 1 K and 1 g kg^{-1}, respectively. The model layers near the surface are typically dryer while the layers above the boundary-layer top are moister with the nonlocal scheme. As a result, the low clouds are shifted upward from the lowest model levels to near 850 mb in the tropics.

The nonlocal scheme utilizes nonlocal transport terms for heat and moisture. From sensitivity studies with the model, we found that a factor-of-two variation in magnitude of the nonlocal transport terms has only a minor influence on the simulations. However, when these terms are removed there is a significant impact. As a part of the nonlocal scheme, the boundary height is diagnosed. Its mean height varies from ~100 m near the South Pole to ~1 km over much of the tropical oceans, and it reaches values larger than 2 km in the storm tracks of the Southern Hemisphere. The diurnal range of the boundary-layer height is small over oceans, but exceeds 4 km over the western Sahara desert.

On the basis of its more comprehensive description of the physics and its important impact, the present nonlocal scheme has been selected for use in CCM2. Long-term climate simulations with CCM2 will be reported elsewhere, as will the formulation and impact of the other changes to the model's physical parameterizations.

Future studies with the nonlocal diffusion scheme may focus on the interaction of the scheme with the hydrological cycle, for example, deep and shallow convection, and the land-surface parameterization. Special consideration may be given to the entrainment process at the top of the boundary layer. Further improvements may consider the influence of entrainment on the scalar mixing (see our discussion in section 3), and consistent treatment of cloud diffusion within the nonlocal scheme.

Acknowledgments. We would like to thank B. Briegleb at NCAR for suggestions and his help with handling data. We also thank our colleagues at KNMI and NCAR for useful comments and discussions, and we acknowledge two unknown referees for their remarks. This work was initiated during a longtime visit of the first author to NCAR, for which he acknowledges financial support.

APPENDIX A

The Turbulent Velocity Scales in the Nonlocal ABL Scheme

The turbulent velocity scale of (3.9) depends primarily on the relative height z/h (h is boundary-layer height) and the stability within the ABL (Holtslag and Nieuwstadt 1986). Here, stability is defined with respect to the surface virtual heat flux $(\overline{w'\theta'_v})_0$, or equivalently with the ratio $h/-L$ [L being the Obukhov length scale, see (A4)]. Second, the velocity scales are also dependent on the specific quantity of interest. We will assume that the velocity scales for mixing of passive scalars and specific humidity are equal to the one for heat, denoted by w_t. For the wind components, the velocity scale is different and denoted by w_m. The specification of w_t and w_m is given in detail by Troen and Mahrt (1986), on the basis of the profile functions of Businger et al. (1971). Holtslag et al. (1990) have rewritten the velocity scale in terms of the more widely accepted profile functions of Dyer (1974) and have given a new formulation for very stable conditions. Below, we follow the latter approach.

For stable ($(\overline{w'\theta'_v})_0 < 0$) and neutral surface conditions ($(\overline{w'\theta'_v})_0 = 0$), the velocity scale for scalar transport is

$$w_t = \frac{u_*}{\phi_h}, \tag{A1}$$

where u_* is the friction velocity defined by

$$u_* = [(\overline{u'w'})_0^2 + (\overline{v'w'})_0^2]^{1/4}. \tag{A2}$$

Furthermore, ϕ_h is the dimensionless vertical temperature gradient given by (Dyer 1974)

$$\phi_h = 1 + 5\frac{z}{L}, \tag{A3}$$

for $0 \leqslant z/L \leqslant 1$. Here, L is the Obukhov length, defined by

$$L = \frac{-u_*^3}{k(g/\theta_{v0})(\overline{w'\theta'_v})_0}. \tag{A4}$$

For $z/L > 1$, Holtslag et al. (1990) propose

$$\phi_h = 5 + \frac{z}{L}, \tag{A5}$$

which matches (A3) for $z/L = 1$. Equation (A5) is a simple means to prevent ϕ_h from becoming too large (and K_c too small) in very stable conditions. This approach is consistent with the stable temperature profiles of Holtslag and De Bruin (1988). In stable conditions, the exchange coefficients for heat and momentum are often found to be similar (e.g., Dyer 1974; Nieuwstadt 1984; Holtslag and De Bruin 1988). Therefore, we may use $w_m = w_t$.

For unstable conditions $(w'\theta'_v)_0 > 0$, we have that w_t and w_m differ in the surface layer ($z/h \leqslant 0.1$) and in the outer layer of the ABL ($z/h > 0.1$). For the surface layer, w_t is given by (A1), with (Dyer 1974)

$$\phi_h = \left(1 - 15\frac{z}{L}\right)^{-1/2}. \tag{A6}$$

Similarly, w_m is written as

$$w_m = \frac{u_*}{\phi_m}, \tag{A7}$$

where ϕ_m is the dimensionless wind gradient given by

$$\phi_m = \left(1 - 15\frac{z}{L}\right)^{-1/3}. \quad \text{(A8)}$$

In the surface layer, the scalar flux is normally given by

$$(\overline{w'c'})_0 = -\frac{ku_*z}{\phi_h}\left(\frac{\partial C}{\partial z}\right). \quad \text{(A9)}$$

Comparison with (3.8) and (3.9) shows that in the surface layer we should have $a = 0$ in (3.10) for consistency.

For the outer layer, w_t and w_m are given by

$$w_t = w_m/\mathrm{Pr}, \quad \text{(A10)}$$

where

$$w_m = (u_*^3 + c_1 w_*^3)^{1/3}, \quad \text{(A11)}$$

and

$$w_* = ((g/\theta_{v0})(\overline{w'\theta'_v})_0 h)^{1/3} \quad \text{(A12)}$$

is the convective velocity scale. Furthermore, Pr is the turbulent Prandtl number, and c_1 is a constant. The latter is obtained by evaluating the dimensionless vertical wind gradient ϕ_m by (A8) at the top of the surface layer, as discussed by Troen and Mahrt (1986). This results in $c_1 = 0.6$. For very unstable conditions ($h \gg -L$ or $w_*/u_* \gg 0$, it can be shown with (A10) that w_m is proportional to $0.85w_*$, while for the neutral case $w_m = u_*$. The turbulent Prandtl number Pr ($=K_m/K_h = w_m/w_t$) of (A10) is evaluated from

$$\mathrm{Pr} = \frac{\phi_h}{\phi_m}\left(\frac{z}{L}\right) + ak\frac{z}{h}\frac{w_*}{w_m} \quad \text{(A13)}$$

for $z = 0.1$ h. Equation (A13) arises from matching (3.8), (3.9), (3.10), and (A9) at the top of the surface layer. As in Troen and Mahrt we assume that Pr is independent of height in the unstable outer layer. Its value decreases from Pr = 1 for the neutral case ($z/L = 0$ and $w_* = 0$) to Pr = 0.6 for $w_*/u_* \approx 10$ in very unstable conditions.

In very unstable conditions, the countergradient term of (3.10) approaches

$$\gamma_c = d\frac{\overline{wC}_0}{w_* h}, \quad \text{(A14)}$$

where $d \approx a/0.85^2$ because for very unstable conditions we obtain $w_m \approx 0.85w_*$. Since, typically, $d \approx 10$ (Troen and Mahrt 1986), we have $a = 7.2$. Similarly, the temperature excess of (3.12) reads in this limit as $d(\overline{w'\theta'_v})_0/w_*$. This leads to $b\ (=0.85d) = 8.5$ in (3.12).

Finally, using the velocity scales in this appendix, the flux equation (3.8) is continuous in relative height (z/h) and in the boundary-layer stability parameter (h/L or w_*/u_*).

APPENDIX B

Time Splitting of the ABL Diffusion Scheme

The vertical diffusion tendency is given by the vertical derivative of the turbulent flux defined in (3.8):

$$\frac{\partial C}{\partial t} = -\frac{1}{\rho}\frac{\partial}{\partial z}[\rho\overline{w'C'}] = \frac{1}{\rho}\frac{\partial}{\partial z}\left[\rho K_c\left(\frac{\partial C}{\partial z} - \gamma_c\right)\right]. \quad \text{(B1)}$$

The vertical diffusion is implemented in CCM2 using a time-split implicit method, as in CCM1. The countergradient term in the nonlocal ABL scheme depends on the surface flux, the boundary-layer depth, and the velocity scale but not explicitly on the diffused quantity. Therefore, the countergradient term cannot be treated implicitly. A forward time difference is used for the diffusion, whereas the leap-frog method is used for the dynamics. This means that the diffusive forward step is over two time steps. The time discretization then results in

$$\frac{C^{n+1} - C^{n-1}}{2\Delta t} = \frac{1}{\rho^{n-1}}\frac{\partial}{\partial z}\left[\rho^{n-1}K_c^{n-1}\left(\frac{\partial C^{n+1}}{\partial z} - \gamma_c^{n-1}\right)\right], \quad \text{(B2)}$$

where subscripts $n-1$ and $n+1$ refer to time levels, with K_c^{n-1} and γ_c^{n-1} evaluated using model variables at time $n-1$. The whole diffusion process is time split from all other processes so that time $n-1$ variables may already have contributions from the dynamics and other physical process. Equation (B2) can be rewritten as

$$C^{n+1} = (1 - 2\Delta t G^{n-1})^{-1}C^* \quad \text{(B3)}$$

$$C^* = C^{n-1} - 2\Delta t H^{n-1}(\gamma_c^{n-1}), \quad \text{(B4)}$$

where G and H are differential operators. There can be a problem in applying (B4) for trace constituents, including water vapor, because these quantities are positive definite. The application of the countergradient term, $H^{n-1}(\gamma^{n-1})$, may result in negative values for C^*, which are not removed by the subsequent implicit diffusion step. This problem is not strictly numerical, it arises under highly nonstationary conditions for which the ABL formulation is not strictly applicable. In practice, we evaluate C^* and check for negative values in the constituent profiles. If a negative value is found, we set $C^* = C^{n-1}$ for that constituent profile (but not for other constituents at the same point). Note that (B3) is just the normal diffusion equation, which is solved using the usual numerical techniques (as in CCM1).

REFERENCES

Beljaars, A. C. M., 1991: Numerical schemes for parametrizations. *Proc. ECMWF Seminar on Numerical Methods in Atmospheric Models.* Vol. II, Reading, U.K., ECMWF, 1–42. [Available from ECMWF, Shinfield Park, Reading RG2 9AX, U.K.]

——, and A. A. M. Holtslag, 1991: Flux parameterization over land surfaces for atmospheric models. *J. Appl. Meteor.*, **30**, 327–341.

Blackadar, A. K., 1962: The vertical distribution of wind and turbulent exchange in neutral atmosphere. *J. Geophys. Res.*, **67**, 3095–3103.

Boville, B. A., 1991: Sensitivity of simulated climate to model resolution. *J. Climate*, **4**, 469–485.

Briegleb, B. P., 1993: Delta-Eddington approximation for solar radiation in the NCAR Community Climate Model. *J. Geophys. Res.*, in press.

Brost, R., and J. C. Wyngaard, 1978: A model study of the stably-stratified planetary boundary layer. *J. Atmos. Sci.*, **35**, 1427–1440.

Businger, J. A., J. C. Wyngaard, Y. Izumi, and E. Bradley, 1971: Flux-profile relationships in the atmospheric surface layer. *J. Atmos. Sci.*, **28**, 181–189.

Deardorff, J. W., 1972: Theoretical expression for the countergradient vertical heat flux. *J. Geophys. Res.*, **77**, 5900–5904.

Dickinson, R. E., 1984: Modeling evapotranspiration for three-dimensional global climate models. *Climate Processes and Climate Sensitivity*, J. E. Hanson and T. Takahashi, Eds., Amer. Geophys. Union, 58–72.

Dyer, A. J., 1974: A review of flux-profile relationships. *Bound.-Layer Meteor.*, **7**, 363–372.

Geleyn, J. F., 1988: Interpolation of wind, temperature, and humidity values from model levels to the height of measurement. *Tellus*, **40A**, 347–351.

Hack, J. J., 1993: Parameterization of moist convection in the NCAR Community Climate Model, CCM2. *J. Climate*, submitted.

Holtslag, A. A. M., and F. T. M. Nieuwstadt, 1986: Scaling the atmospheric boundary layer. *Bound.-Layer Meteor.*, **36**, 201–209.

——, and H. A. R. de Bruin, 1988: Applied modelling of the nighttime surface energy balance over land. *J. Appl. Meteor.*, **22**, 689–704.

——, and A. C. M. Beljaars, 1989: Surface flux parameterization schemes: Developments and experiences at KNMI. *Proc. ECMWF Workshop on Parameterization of Fluxes over Land Surface*, ECMWF, 121–147. [Also available as KNMI Sci. Rep. 88-06, De Bilt NL, 27 pp.]

——, and C.-H. Moeng, 1991: Eddy diffusivity and countergradient transport in the convective atmospheric boundary layer. *J. Atmos. Sci.*, **48**, 1690–1698.

——, E. J. F. de Bruijn, H.-L. Pan, 1990: A high resolution air mass transformation model for short-range weather forecasting. *Mon. Wea. Rev.*, **118**, 1561–1575.

Holzworth, G. C., 1964: Estimates of mean maximum mixing depths in the contiguous United States, *Mon. Wea. Rev.*, **92**, 235–242.

Kiehl, J. T., 1991: Modelling and validation of clouds and radiation in the NCAR Community Climate Model (CCM2). *Proc. ECMWF/WCRP Workshop on Clouds, Radiative Transfer and the Hydrologic Cycle*, ECMWF, 249–272. [Available from ECMWF, Shinfield Park, Reading RG2 9AX, U.K.]

Louis, J. F., 1979: A parametric model of vertical eddy fluxes in the atmosphere. *Bound.-Layer Meteor.*, **17**, 187–202.

——, M. Tiedtke, and J. F. Geleyn, 1982: A short history of the PBL parameterization at ECMWF. *Proc. ECMWF Workshop on Boundary-Layer Parameterization*, ECMWF, 59–79. [Available from ECMWF, Shinfield Park, Reading RG2 9AX, U.K.]

McFarlane, N. A., 1987: The effect of orographically excited gravity wave drag on the general circulation of the lower stratosphere. *J. Atmos. Sci.*, **44**, 1775–1800.

Mahrt, L., 1976: Mixed layer moisture structure. *Mon. Wea. Rev.*, **104**, 1403–1407.

Mellor, G. L., and T. Yamada, 1974: A hierarchy of turbulence closure models for planetary boundary layers. *J. Atmos. Sci.*, **31**, 1791–1806.

Nieuwstadt, F. T. M., 1984: Some aspects of the turbulent stable boundary layer. *Bound.-Layer Meteor.*, **30**, 31–55.

O'Brien, J. J., 1970: A note on the vertical structure of the eddy exchange coefficient in the planetary boundary layer. *J. Atmos. Sci.*, **27**, 1213–1215.

Pan, H.-L., 1990: A simple parameterization scheme of evapotranspiration over land for the NMC medium-range forecast model. *Mon. Wea. Rev.*, **118**, 2500–2512.

Rasch, P. J., and D. L. Williamson, 1990: Computational aspects of moisture transport in global models of the atmosphere. *Quart. J. Roy. Meteor. Soc.*, **116**, 1071–1090.

Shea, D. J., K. E. Trenberth, R. W. Reynolds, 1990: A global monthly sea surface temperature climatology. NCAR Tech. Note, NCAR/TN-345+STR, 167 pp.

Simmons, A. J., and R. Strüfing, 1983: Numerical forecasts of stratospheric warming events using a model with a hybrid vertical coordinate. *Quart. J. Roy. Meteor. Soc.*, **109**, 81–111.

Slingo, J. M., 1987: The development and verification of a cloud prediction scheme for the ECMWF model. *Quart. J. Roy. Meteor. Soc.*, **113**, 899–927.

Stull, R. B., 1991: Static stability: An update. *Bull. Amer. Meteor. Soc.*, **72**, 1521–1529.

Troen, I., and L. Mahrt, 1986: A simple model of the atmospheric boundary layer: Sensitivity to surface evaporation. *Bound.-Layer Meteor.*, **37**, 129–148.

Williamson, D. L., J. T. Kiehl, V. Ramanathan, R. E. Dickinson, and J. J. Hack, 1987: Description of NCAR Community Climate Model (CCM1), NCAR Tech. Note, NCAR/TN-285+STR, 112 pp.

Wyngaard, J. C., and R. A. Brost, 1984: Top-down and bottom-up diffusion of a scalar in the convective boundary layer. *J. Atmos. Sci.*, **41**, 102–112.